IEEE Access
Multidisciplinary | Rapid Review | Open Access Journal

Received July 13, 2020, accepted July 30, 2020, date of publication August 10, 2020, date of current version August 20, 2020.

Digital Object Identifier 10.1109/ACCESS.2020.3015335

3D-Printed UHF-RFID Tag for Embedded Applications

NEUS VIDAL[1], JOSEP MARIA LOPEZ-VILLEGAS[1], (Senior Member, IEEE), JORDI ROMEU[2], (Fellow, IEEE), ARNAU SALAS BARENYS[1], ALEIX GARCIA-MIQUEL[1], GISELLE GONZÁLEZ-LÓPEZ[2], AND LUIS JOFRE[2], (Fellow, IEEE)

[1]Department of Electronic and Biomedical Engineering, University of Barcelona (UB), 08028 Barcelona, Spain
[2]Department of Signal Theory and Communications, CommSensLab, Universitat Politècnica de Catalunya (UPC), 08034 Barcelona, Spain

Corresponding author: Neus Vidal (nvidal@ub.edu)

This work was supported by the Spanish Ministry of Economy and Competitiveness, under Project TEC2017-83524-R, Project TEC2016-78028-C-1P, and Project MDM2016-0600.

ABSTRACT This paper presents the design, manufacture and characterization of a novel 3D passive UHF-RFID tag for embedded applications. The prototype is fabricated using additive manufacturing techniques: 3D printing and copper electroplating. The design, manufacturing process and measurement set-up are presented and discussed in detail. We propose a biconical antenna design with spiral strips embedded in the cones to provide compactness without breaking the symmetry of the component and to improve bandwidth. The antenna is matched to a commercial UHF-RFID integrated circuit. We incorporate a packaging design that consists of a dielectric coating, to provide proper operation in different media or surrounding environments with changing electromagnetic properties. The good agreement between experimental results and Finite Element Method simulations allows us to validate the whole process. Finally, a compact capsule-type RFID tag is proposed and its performance in different media is reported.

INDEX TERMS 3D printing, UHF RFID tag, embedded antenna, antenna design, packaging.

I. INTRODUCTION

The use of additive manufacturing (AM) techniques to improve the performance of integrated antenna systems has huge potential. Recently published Special Issues on manufacturing techniques and 3D-printing technology for advanced and novel antenna applications suggest the future impact of this technology [1], [2]. By adopting 3D-printing techniques, we can escape from planarity and produce models that may allow increased compactness and whole system integration, while maintaining electrical performance. An example of an application where compactness and system performance improvement can be of considerable benefit is radio-frequency identification (RFID) technology.

Due to its cost-effectiveness and low power consumption electronics, passive RFID technology is widely used in many industrial applications such as tracking, access control, logistics, etc. [3]. However, there are still important limitations to this technology. One related challenge is making the antenna design sufficiently robust to allow proper operation in a surrounding environment with changing electromagnetic properties. If this requirement is not met, variations in antenna impedance may produce a mismatch and therefore a reduction in the RFID chip activation range. This is critical when dealing with lossy media such as liquids or biological tissues [4]. Hospitals are one example where the impact of the surrounding lossy media (medical personal, patients) can produce a decrease in the radiative efficiency of RFID tags [5].

A second challenge in the design of antennas for RFID applications is ensuring that the RFID tag can work not only close to heterogeneous or lossy media, but also immersed in them. In the literature, we can find case studies of fully embedded RFIDs for application in some industries, such as the automotive and construction sectors [6]–[8]. These report limitations of RFID tag operation, mainly due to the impact of external conditions. It is not only a question of the effect of electrical losses related to the specific medium, but also the time variability of the whole set of electrical properties. An antenna immersed in a certain medium must be able to operate properly, to the maximum extent, regardless of changes in the dielectric constant and conductivity. This does not only mean that it must exhibit good matching throughout a certain range of values, but also that it should respond adequately to temporal variations.

The associate editor coordinating the review of this manuscript and approving it for publication was Nosherwan Shoaib.

Another important aspect, which depends on the operating frequency, is the space distribution of the antenna field regions, as they substantially modify the behavior of the radiated power. The reactive near-field region has a great impact on the behavior of the radiated power of the antenna, as reported in [9]. The presence of lossy media dramatically decreases the radiative efficiency of the antenna, because they interact with the reactive near-field.

Packaging antennas is a potential way to resolve these issues that has already been proposed in previous studies [10]. Dielectric encapsulation to guarantee stable antenna impedance when immersed in a dielectric medium was validated through numerical simulations; and packaging can be designed to minimize changes in antenna reactance. Moreover, keeping the reactive near-field inside the coating minimizes the impact of medium losses on radiative efficiency [9], [11].

In accordance with all these considerations, in this work, we present the design and characterization of a compact 3D-printed passive UHF-RFID tag for embedded applications. Different designs and technologies have been proposed for 3D-printed antennas [1], [2], [12], [13]. Here, we present a novel biconical spiral antenna design, including a dielectric coating that acts as an electromagnetic buffer. The prototype is fabricated using AM techniques: material-jetting 3D printing and cooper electroplating. The antenna design specifications are set to match the input impedance of a commercial UHF-RFID integrated circuit.

The paper is organized as follows. In Section II, we explain the methodology, including the antenna design procedure and manufacturing process. Due to its importance, a whole section (Section III) is devoted to the measurement set-up. In Section IV, the electromagnetic simulations and experimental results are presented and discussed. Finally, Section V presents our main conclusions.

II. ANTENNA DESIGN AND MANUFACTURE

A. DESIGN OF THE 3D ANTENNA

The 3D antenna we designed consists of two main symmetrical radiators, a matching network, and a dielectric coating. The antenna body is a biconical structure with a square plate in the middle, perpendicular to the cone axes, implemented in a dielectric material whose electromagnetic (EM) parameters are: dielectric constant, 2.8 and loss tangent, 0.02. Due to the antenna geometry, we proposed a cylindrical coating. Figure 1 shows a view of the computer-assisted design (CAD) models.

EMPro from Keysight Technologies Inc. was used as the design and simulation environment. The radiators were defined on the external surface of the cones, as outer metal conical sections connected to the middle plate via a conical metal spiral. The matching network is implemented in the middle plate as an inductive transformer. Two square metal loops were defined using metal strips on both sides of the plate and a via hole. This configuration allows broadband matching of the antenna impedance to that of the RFID chip.

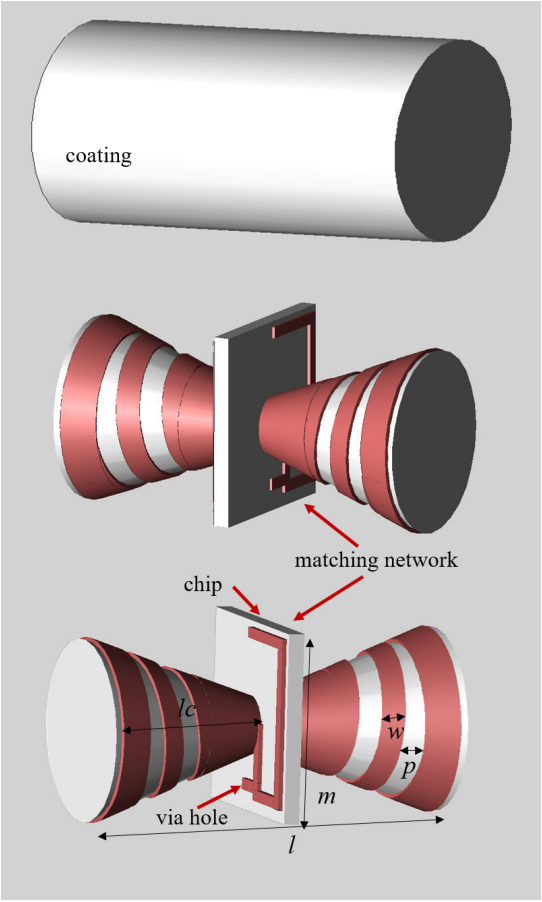

FIGURE 1. 3D view of the coating and the helical antenna design. The matching network located at each side of the perpendicular plate is shown. The via hole and chip locations are indicated. Main design parameters are labeled.

All the metal parts are partially buried inside the dielectric material (i.e., to half its thickness). This is a step required by the manufacturing process that will be discussed in detail in the next section. Finally, the coating is a cylinder that completely encloses the antenna, implemented using the same dielectric material as the body of the antenna. It is used as a buffer to minimize detuning effects due to variations in the EM properties of the surrounding environment.

The main design parameters are: l, the total length of the antenna; α, the cone angle; lc, the width of the conical sections of the radiators; w, the width of the metal trace in the conical spiral; p, the pitch between turns in the conical spiral; and the perimeter and surface of the square loops of the matching network. There are some constraints on these parameters to reduce the dimensions of the design space. For instance, an arbitrary choice of l, lc, w, and p, may lead to impossible geometries, and so unpractical antennas.

We used EM simulation tools based on the Finite Element Method (FEM) to evaluate the response of the antenna in terms of the differential reflection coefficient. This allows for optimization of the antenna design, to fulfill the target specifications. In practice, the right selection of the design parameters leads to antenna designs tuned to the desired operating

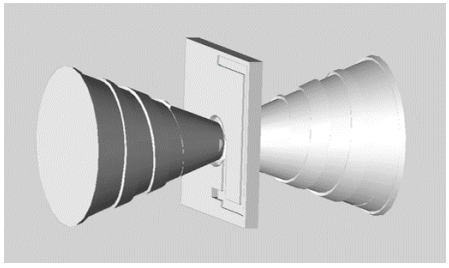

FIGURE 2. View of the final spiral antenna CAD file.

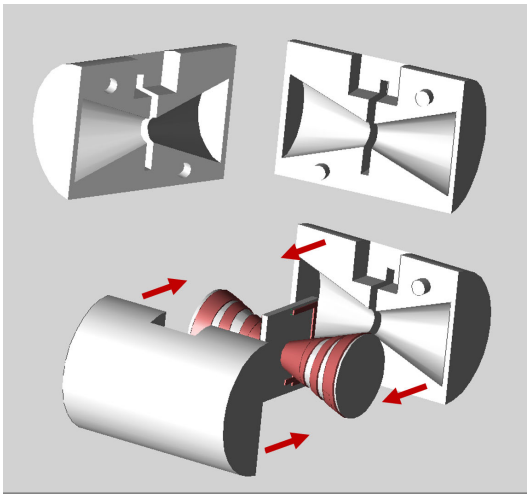

FIGURE 3. View of the final coating CAD files.

frequency and impedance of the RFID chip. Compact designs can also be achieved at the expense of antenna bandwidth.

B. MANUFACTURING PROCESS

The manufacturing process consisted of two groups of tasks that implement the transition from CAD (i.e., the optimized antenna design) to the final part (i.e. the actual component). The first group includes all the virtual tasks and is performed inside the design environment. After the optimized antenna design is obtained, all the simulation ports and field sensors are discarded. All the metal parts as well as all the dielectric parts are combined using Boolean operators into two single objects. Then the metal object is subtracted from the dielectric object to form the printable part. An example of the final result can be observed in Figure 2. The printable part is basically the main body of the antenna with trenches on the surface and via hole where the metal parts are located. This is a consequence of the fact that during the design phase the metal parts are partially buried inside the dielectric material. This group of virtual tasks finishes when the printable CAD object is coded in the appropriate format for 3D printing.

To manufacture the dielectric coating, the main body of the antenna is first subtracted from the dielectric cylinder using Boolean operators. Then, the resulting object is cut into two halves. Finally, after adding alignment features, the resulting structures are ready for 3D printing. An example is shown in Figure 3.

FIGURE 4. View of the final printed coated antenna.

The second group of tasks is related to the printing of the parts. The coating halves are printed directly. For the antenna, the first task consists of spraying the object with a silver ink [14] to form a conductive coating. Then the silver is removed from areas where it is not wanted by polishing so that the silver ink only remains in the trenches of the conical surface, on the middle plate and in the via hole. The remaining silver ink is conductive enough to serve as a seed for a standard copper electroplating process. The role of the silver ink is merely to serve as the seed onto which the copper electroplating layer grows. Any similar conductive ink could be used as the seed. The only effect of the conductivity of the seed is observed at the beginning of cooper growth, and particularly on the initial growth rate until an effective copper layer is present. After that, the growth does not depend on the seed at all.

The result is the final part, corresponding to the optimized antenna design. An example is shown in Figure 4. It is worth noting that the same manufacturing procedure has been successfully used to implement helical-microstrip transmission lines [15], and conical inductors with improved bandwidth [16]. This last reference includes a full explanation and a visual description of the virtual and physical tasks of the process flow for the design and 3D manufacturing.

III. MEASUREMENT SET-UP

To validate the design and manufacturing process of the antenna prototypes, it was necessary for us to compare FEM simulation and experimental results. Accordingly, we needed to measure the differential reflection coefficient of the antenna. Using a standard Vector Network Analyzer (VNA), this requires a transformation from single-ended to differential excitation. To achieve this goal, electrical and electro-optical converters have been proposed. In our case, we used an electrical transformer that incorporates, as a key component, a miniaturized balun NCS4-102+ from Mini-Circuits [17]. We chose this component because its amplitude and phase unbalance are minimal at the operating frequency of the RFID chip (i.e., 0.05 dB and 0.04 degrees at 868 MHz, respectively).

The transformer was implemented using a printed circuit board (PCB). The layout is shown in Figure 5a. On the

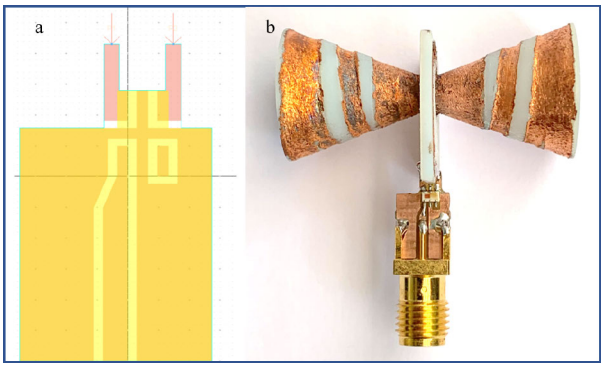

FIGURE 5. a) View of the electrical converter layout. b) Antenna prototype with the single ended to differential converted connected.

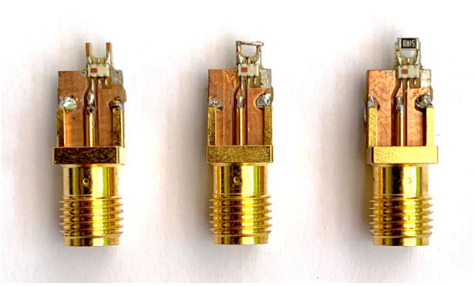

FIGURE 6. View of the calibration kit used to de-embed the effect of SMA connectors and pads. From left to right: open, short, and load.

bottom of the PCB we can observe pads for soldering an edge lunch SubMiniature version A (SMA) connector where the single-ended excitation is applied. In the middle are the pads for soldering the balun. Finally, on top, we can see two pins corresponding to the differential excitation applied to the antenna prototype. Figure 5b shows a sample antenna prototype with the single-ended to differential converter connected at the same location where the RFID chip is to be soldered.

It is important to note that prior to the measurements the VNA must be calibrated properly. This requires a custom calibration kit to be able to de-embed all the effects of the converter, other than the single-ended to differential conversion, from the S parameter measurement; for instance, it is necessary to de-embed insertion loss or impedance mismatch. We designed and manufactured the custom calibration kit using the same procedure as for the single-ended to differential converter. In practice, open, short, and broadband load standards were implemented by connecting the corresponding impedances between the differential pins of three converters. A view of the calibration kit is shown in Figure 6. With this custom calibration kit, the differential reflection coefficient of the antenna prototypes was measured in the range from 700 MHz to 1 GHz using an E5071C 4-port VNA from Keysight Technologies Inc.

IV. RESULTS AND DISCUSSION

A. FINAL DESIGN OF THE ANTENNA AND THE COATING

The production of the final model (antenna plus coating) consisted of different stages. The first was to design the antenna without the coating. The response in terms of the differential reflection coefficient, efficiency and bandwidth was evaluated. A set of antennas were designed and fabricated. We started with a biconical antenna design and introduced the spiral layout, then progressive miniaturization was performed. We varied the α, p and w parameters to obtain the smallest prototype that met the target specifications. Changes in α and w were not critical, similar results were obtained when changing the angle and the section of the radiator. The pitch between turns in the conical spiral was the key parameter: reducing p yielded a compact design, but also produced a major reduction in both efficiency and bandwidth. Table 1 presents the results for 4 different prototypes: the conical reference antenna and 3 spiral antennas. The design we finally selected and which is presented in the previous sections (antenna number 3 in Table 1) offers a compromise between size, bandwidth, and system efficiency. From this point on, all further compaction of the antenna resulted in a drastic bandwidth reduction and a decrease in efficiency (antenna number 4 in Table 1). Once the final design was chosen, we added the coating and readjusted the antenna size in accordance with the change in permittivity.

TABLE 1. Antenna prototypes without coating.

Antenna	Total Length (mm)	Radiation Efficiency (%)	Bandwidth (MHz)
1 	96	99	90-100
2 	52	96.6	60-90
3 	42.5	74.9	40-60
4 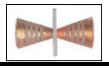	29.9	61.6	15-20

The second stage was related to the coating design, for which we considered previous theoretical work [10]. Those authors showed how proper packaging can minimize changes in the antenna reactance due to differences in the surrounding dielectric medium. They also demonstrated that packaging with a radius of 0.1λ contains most of the stored reactive energy and provides impedance stability. Consequently, we defined an initial radius for the cylinder of 20.65 mm (0.1λ at 868 MHz for the ε_r of the material). To test the effectiveness of this approach, we modeled the performance of our coated antenna when immersed in different media. From this point, antenna and packaging were always modelled and retuned simultaneously.

We chose media with different extreme electrical permittivity and conductivity: fat, cancellous bone, brain, and water. The dielectric properties of these media were taken from [18] and the values are listed in Table 2. The dielectric permittivity ranges from 1 to 84.5. Our results agreed with the previous theoretical analysis [10] and showed the expected behavior. The coating was an effective buffer that minimized the impact

TABLE 2. Electrical properties.

Symbol	Relative Permittivity	Loss Tangent
Reference	1	0
Fat	11.3	0.2
Cancellous Bone	20.9	0.32
Brain	57	0.6
Water	84.5	0.042

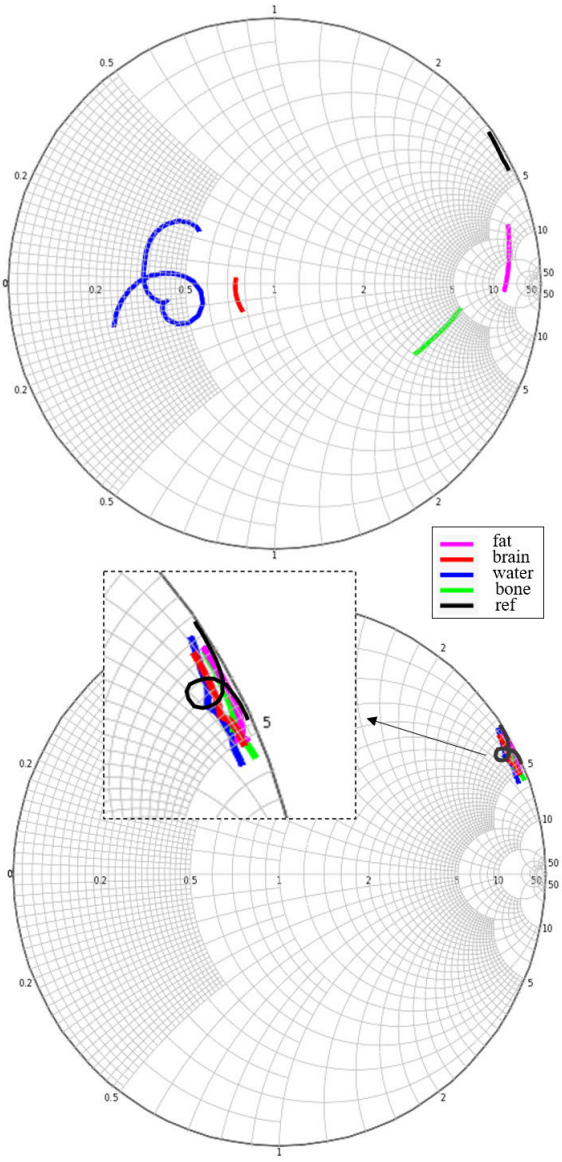

FIGURE 7. Results for the antenna Impedance from 0.75 GHz to 0.9 GHz; a) without coating and b) with coating. Tag is immersed in fat, cancellous bone, brain and water.

of the changing environment on antenna performance. At this point, to analyze possible further compactness of the coating, we progressively tested the impact of a reduction of its radius. Good results were also obtained for a radius of 0.06λ, so we kept this value for the final model.

Figure 7 (top) shows the simulated response of the RFID tag when immersed in different media. For purposes of comparison with previous published results (10), the reference impedance of the Smith Chart was set to 50 Ω. At the bottom of Figure 7, the same results are shown when the antenna is covered with the coating. In both cases, the behavior is analyzed for frequencies in the range from 0.75 to 0.95 GHz. We can observe that the input impedance of the antenna varies greatly when it is immersed in different media, while the values change only slightly when the coating is added. This demonstrates the effectiveness of the coating at stabilizing the antenna impedance, regardless of variation in the EM properties of the surrounding medium. The effect of the dielectric coating on the radiative characteristics of the tag antenna is analyzed in the next section.

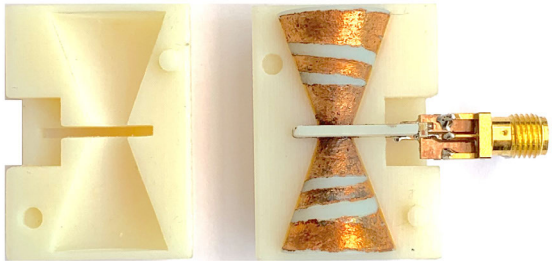

FIGURE 8. View of the final antenna prototype and coating, mounted and ready for EM characterization.

TABLE 3. Dimensions of the prototype.

Symbol	Quantity	Value
l	Total length	33.6 mm
α	Cones angle	20 °
lc	Length conical sections	16.1 mm
m	Metal trace width	2 mm
r	Coating radius	13 mm
cl	Coating length	36 mm
V	Capsule volume	191.13 cm^3

B. TAG RESULTS

Considering all the previous analysis and results, a final prototype was designed, fabricated, and tested. A view of the resulting antenna and coating is shown in Figure 8. To carry out the S11 parameter measurements, an opening was made in the coating. This allowed connection of the single-ended to differential converter (also shown in the figure) to the antenna. All the dimensions of the prototype, including antenna and coating, are indicated in Table 3.

The reflection coefficient of the prototype in the frequency band of interest is shown in Figure 9. The figure compares the simulation results obtained using FEM with the experimental measurements after de-embedding the effect of the single-ended to differential converter. Good agreement is observed between the experimental results and the FEM simulations, especially if we consider that the simulations were carried out using a true differential port while the measurements required the use of the single-ended to differential converter and a de-embedding procedure. In any case, we did observe some discrepancies, especially in

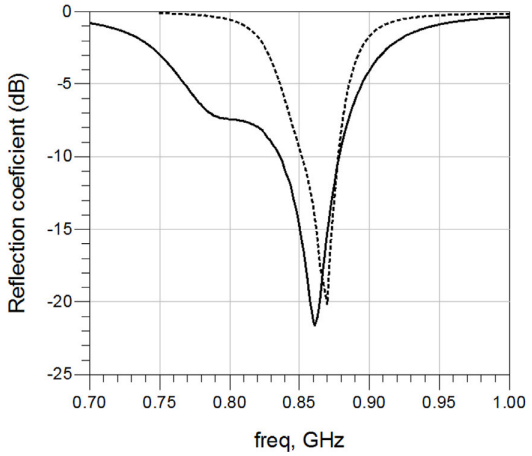

FIGURE 9. Simulated (dotted line) and measured (continuous line) reflection coefficient of the tag on air.

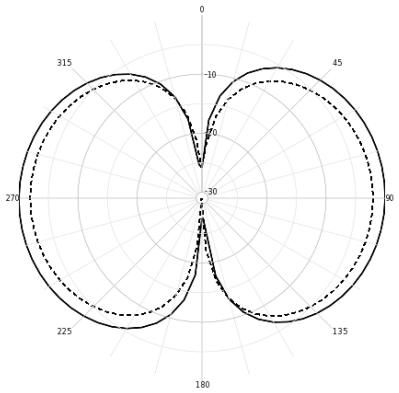

FIGURE 10. Polar cut of the radiation gain as a function of theta for phi=0: results of the final tag antenna without coating (continuous line) and with coating (dotted line).

the bandwidth. These discrepancies have two main origins. The first is the effect of printing tolerances. The printing accuracy is about 60 μm in the XY-plane and, 16 μm along the Z-axis. Considering the complexity of the geometry, this leads to a variable accuracy throughout the whole structure that is reflected in its electromagnetic behavior. This is particularly important for the most sensitive parts of the design, such as the matching network or the spirals. The second is related to possible variation of the electrical permittivity of the base structure. In the figure we can observe that the measured resonant frequency of the prototype is 860 MHz: a deviation of 8 MHz from the target value of 868 MHz. Concerning the antenna bandwidth at -10 dB, the values obtained are 26 MHz (FEM) and 39 MHz (experimental). This bandwidth offers enough compensation for detuning effects resulting from the tolerances of the manufacturing process.

Concerning the radiative properties of the coated antenna prototype, the simulated system efficiency was 42.18% at 868 MHz. The value without the coating was 74.9% (Table 1). The gain decreased from 0.34 dB to -2.99 dB. Finally, the impact of the coating on the radiation pattern is plotted on Figure 10.

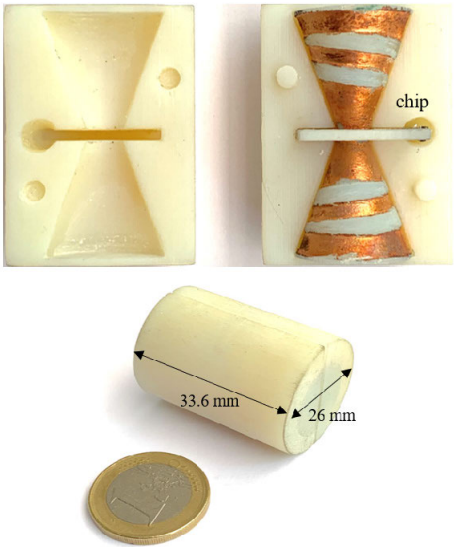

FIGURE 11. View of the final UHF-RFID Tag capsule.

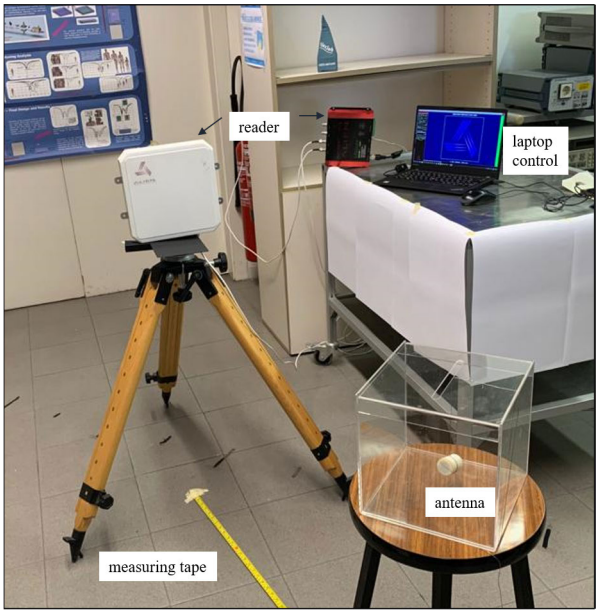

FIGURE 12. View of the RFID read-range measurement setup.

After validating the antenna design and the effectiveness of the dielectric coating, we considered the integration of the RFID IC to implement a fully functional device. In this case, the RFID IC was the Higgs 3 from Alien Technology, with a power threshold sensitivity of -15/-17 dBm. The input impedance of this component was used as a reference throughout the whole design process to match the antenna impedance. The final UHF-RFID tag capsule is shown in Figure 11: it has a volume of 191.13 cm^3 (length 36 mm, radius 13 mm). To evaluate the performance of the prototype, a commercial "Alien ALR-9900+" [19] reader was used. The set-up for measuring the RFID read-range is shown in Figure 12. The reader antenna was secured on a tripod aligned with the tag. The tag was fixed via a plastic wire

inside a methacrylate box. A measuring tape was placed on the floor. The tag measurements started at 0.5 m from the reader. Control software allowed us to check the reader–tag connectivity on the laptop. The tag was covered with a plastic film to waterproof the electronic components. First, the measurements were performed in air, and a read range of 4.5 m was obtained, which is coherent with the sensitivity of the chip (-15/-17 dBm). Then the tag was tested immersed in water and we obtained a 60% reduction in the range of the communication link. This agrees with EM simulations that account for losses in water, and validates the communication capabilities of the proposed tag.

V. CONCLUSION

In this work we present the design, manufacturing process, and results of experimental characterization of a 3D-printed passive UHF-RFID tag for embedded applications. We adopt a biconical geometry with 3D spirals on its surfaces to increase compactness. Geometrical parameters, such as the cone angle, distance between the metal strips and their dimensions, were analyzed to reduce the overall size of the prototype while maintaining, as far as possible, its frequency tuning, impedance matching and communication capabilities. Packaging consisting of a dielectric coating was added to minimize impedance changes when the antenna is immersed in different dielectric media. Initially, simulations were carried out to assess the impedance matching, in terms of the reflection coefficient, and the operational range of the antenna. Then we analyzed the coating. A specific cylindrical design was suggested, to contain most of the stored reactive energy and provide proper operation in different media or in environments with changing electromagnetic properties. The system was tested when immersed in different extreme materials, including air, water, and biological tissues.

After validating the design process, a tag prototype was fabricated using additive manufacturing techniques: 3D printing and copper electroplating. A specific measurement set-up was implemented to accurately measure the differential response of the antenna prototype. Finally, a fully functional compact UHF-RFID tag was assembled combining the antenna, the dielectric coating, and a commercial RFID IC. The results demonstrate the feasibility and good performance of the system. The coated 3D-printed antenna for RFID applications shows promising behavior in the UHF-RFID band for embedded applications. Sectors such as the construction industry, motor industry and healthcare, among others, could benefit from the use of tags that minimize the impact of external conditions and lossy media.

ACKNOWLEDGMENT

The authors would like to thank Alien Technologies for providing the IC.

REFERENCES

[1] "Guest Editorial: Microwave components and antennas based on advanced manufacturing techniques," *IET Microw., Antennas Propag.*, vol. 11, no. 14, pp. 1919–1920, Nov. 2017, doi: 10.1049/iet-map.2017.1007.
[2] S. K. Sharma, H. Xin, B.-I. Wu, J. C. Vardaxoglou, and C. H. Chan, "Guest editorial special cluster on three-dimensional printed antennas and electromagnetic structures," *IEEE Antennas Wireless Propag. Lett.*, vol. 17, no. 11, pp. 1998–2002, Nov. 2018.
[3] K. Jung and S. Lee, "A systematic review of RFID applications and diffusion: Key areas and public policy issues," *J. Open Innov. Technol., Market, Complex.*, vol. 1, no. 1, pp. 1–19, Dec. 2015.
[4] G. Deschamps, "Impedance of an antenna in a conducting medium," *IRE Trans. Antennas Propag.*, vol. 10, no. 5, pp. 648–650, Sep. 1962.
[5] W. Yao, C.-H. Chu, and Z. Li, "The use of RFID in healthcare: Benefits and barriers," in *Proc. IEEE Int. Conf. RFID-Technol. Appl.*, Jun. 2010, pp. 128–134.
[6] S. Basat, M. M. Tentzeris, and J. Laskar, "Design and development of a miniaturized embedded UHF RFID tag for automotive tire applications," in *Proc. IEEE Int. Workshop Antenna Technol. Small Antennas Novel Metamater.*, Lake Buena Vista, FL, USA, vol. 1, May/Jun. 2005, pp. 867–870.
[7] S.-H. Jeong and H.-W. Son, "UHF RFID tag antenna for embedded use in a concrete floor," *IEEE Antennas Wireless Propag. Lett.*, vol. 10, pp. 1158–1161, 2011.
[8] J.-M. Laheurte, A. Kabalan, H. Retima, E. Piedallu, F. Michelis, and B. Lebental, "Embedded UHF RFID tag for durability monitoring in concrete," *Wireless Sensor Netw.*, vol. 8, no. 7, pp. 137–144, 2016.
[9] A. K. Skrivervik, "Implantable antennas: The challenge of efficiency," in *Proc. 7th Eur. Conf. Antennas Propag. (EuCAP)*, Apr. 2013, pp. 3627–3631.
[10] J. Romeu, G. Gonzalez-Lopez, S. Blanch, and L. Jofre, "Antenna packaging for in-body applications," in *Proc. 14th Eur. Conf. Antennas Propag. (EuCAP)*, Copenhagen, Denmark, Mar. 2020, pp. 1–5.
[11] A. K. Skrivervik and F. Merli, "Design strategies for implantable antennas," in *Proc. Loughborough Antennas Propag. Conf.*, Nov. 2011, pp. 1–5.
[12] J. Bjorgaard, M. Hoyack, E. Huber, M. Mirzaee, Y.-H. Chang, and S. Noghanian, "Design and fabrication of antennas using 3D printing," *Prog. Electromagn. Res. C*, vol. 84, pp. 119–134, 2018.
[13] M. Liang, J. Wu, X. Yu, and H. Xin, "3D printing technology for RF and THz antennas," in *Proc. Int. Symp. Antennas Propag. (ISAP)*, Okinawa, Japan, Oct. 2016, pp. 536–537
[14] *Silver Adhesive Conductive Paint*. Accessed: May 30, 2020. [Online]. Available: https://docs.rs-online.com/d712/0900766b815139c0.pdf
[15] J. M. Lopez-Villegas, A. Salas, and N. Vidal, "Modeling of 3-D-printed helical-microstrip transmission lines for RF applications," *IEEE Trans. Microw. Theory Techn.*, vol. 67, no. 12, pp. 4914–4921, Dec. 2019.
[16] J. M. Lopez-Villegas, N. Vidal, J. Sieiro, A. Salas, B. Medina, and F. M. Ramos, "Study of 3-D printed conical inductors for broadband RF applications," *IEEE Trans. Microw. Theory Techn.*, vol. 66, no. 8, pp. 3597–3602, Aug. 2018.
[17] *Ceramic Balun RF Transformer*. Accessed: May 30, 2020. [Online]. Available: https://www.minicircuits.com/pdfs/NCS4-102+.pdf
[18] C. Gabriel, "Compilation of the dielectric properties of body tissues at RF and microwave frequencies," Occupational Environ. Health Directorate, Radiofrequency Radiat. Division, Brooks Air Force Base, San Antonio, Texas, USA, Tech. Rep. N.AL/OE-TR-1996-0037, 1996.
[19] *Alien Technology Readers*. Accessed: Mar. 18, 2020. [Online]. Available: http://www.alientechnology.com/products/readers/

NEUS VIDAL received the Ph.D. degree in physics from the University of Barcelona, Spain, in 1995. She is currently an Associate Professor with the University of Barcelona, where she is also a member of the Group of Excellence for Radio Frequency Components and Systems. Her current research interests include antenna design for biomedical applications and electromagnetic propagation-related issues.

JOSEP MARIA LOPEZ-VILLEGAS (Senior Member, IEEE) received the Ph.D. degree in physics from the University of Barcelona, Barcelona, Spain, in 1990. He is currently the Director of the Group of Excellence for Radio Frequency Components and Systems, University of Barcelona, where he is also a Full Professor with the Department of Electronic and Biomedical Engineering. His research interests include the design, optimization, and test of RF components, circuits and systems performed using silicon, multilayered technologies, such as multichip modules and low-temperature co-fired ceramics, 3D printing, the use of 3-D simulators for electromagnetic analysis of RF components, circuits and systems, the analysis of electromagnetic compatibility and electromagnetic interference problems, and the interaction of electromagnetic energy with biological tissues. He is particularly interested in the modeling and optimization of integrated inductors and transformers for general RF applications, and in particular for the development of new homodyne transceiver architectures based on injection-locked oscillators.

JORDI ROMEU (Fellow, IEEE) was born in Barcelona, Spain, in 1962. He received the Ingeniero de Telecomunicación and Doctor Ingeniero de Telecomunicaciòn degrees from the Universitat Politècnica de Catalunya (UPC), in 1986 and 1991, respectively. In 1985, he joined the Antennalab, Signal Theory and Communications Department, UPC, where he is currently a Full Professor and involved in antenna near-field measurements, antenna diagnostics, and antenna design. He was a Visiting Scholar at the Antenna Laboratory, University of California at Los Angeles, Los Angeles, in 1999, on an NATO Scientific Program Scholarship, and at the University of California at Irvine, in 2004. He holds several patents and has published 60 refereed articles in international journals and 80 conference proceedings. He was a Grand Winner of the European IT Prize, awarded by the European Commission, for his contributions in the development of fractal antennas, in 1998. More information can be found in http://www.researchgate.net/profile/Jordi_Romeu.

ARNAU SALAS BARENYS received the B.E. degree in electronics engineering of telecommunication from the Universitat de Barcelona (UB), Spain, and the M.S. degree in telecommunication engineering from the Universitat Autònoma de Barcelona (UAB), Spain, in 2017. He is currently pursuing the Ph.D. degree in engineering and applied science with UB. His research interests include electronics design, radiofrequency and electromagnetic modelling, communication systems, 3D design, and 3D printing.

ALEIX GARCIA-MIQUEL received the M.Sc. degree in telecommunication engineering from the Universitat Politècnica de Catalunya (UPC), Barcelona, Spain, in 2009, and the M.Sc. and Ph.D. degrees in biomedical engineering from the Universitat de Barcelona (UB), Barcelona, in 2013 and 2018, respectively. Since 2012, he has been collaborating with the Radiofrequency Group (GRAF), Electronics and Biomedical Engineering Department, UB, as an Assistant Professor and then as an External Collaborator. He has been involved in a wide range of positions, from multinational corporations to start-ups. His current research interests include antenna design, medical devices development, fetal medicine, and management of multidisciplinary teams.

GISELLE GONZÁLEZ-LÓPEZ was born in Havana, Cuba, in 1992. She received the B.S. degree in telecommunication and electronics engineering from Technical University ISPJAE, Havana, in 2015, and the M.S. degree in telecommunication engineering from the Technical University of Catalonia (UPC), Barcelona, in 2018. She is currently pursuing the Ph.D. degree with the Signal Theory and Communications (TSC) Department, Research Group of Remote Sensing, Antennas, Microwaves and Superconductivity, Unidadde Excelencia Maria de Maeztu, UPC. From 2016 to 2017, she was an Intern at the Research Group of Mobile communications (GRCM), UPC. Her research interests include but are not limited to embedded systems, media characterization, microwave antenna design, antenna impedance characterization, wireless communications, and mobile systems.

LUIS JOFRE (Fellow, IEEE) received the M.Sc. and Ph.D. degrees in electrical engineering (telecommunication engineering) from the Universitat Politècnica de Catalunya (UPC), Barcelona, Spain, in 1978 and 1982, respectively. Since 1982, he has been with the Communications Department, Telecommunication Engineering School, UPC, as an Associate Professor and then has been a Full Professor, since 1989. He was also a Visiting Professor at the Ecole Supèrieure d'Electricitè Paris, from 1981 to 1982, where he was involved in microwave antenna design and imaging techniques for medical and industrial applications. From 1986 to 1987, he was a Visiting Fulbright Scholar with the Georgia Institute of Technology, Atlanta, GA, USA, where he was involved in antenna near-field measurements and electromagnetic imaging. From 2000 to 2001, he was a Visiting Professor with the Electrical and Computer Engineering Department, Henry Samueli School of Engineering, University of California at Irvine, CA, USA, where he was involved in reconfigurable antennas and microwave sensing of civil engineering structures. He has been the Director of the UPC-Telefonica Chair on Information Society Future Trends, since 2003. He was a Principal Investigator of the 2008–2013 Spanish Terahertz Sensing Lab Consolider Project, the Research Leader of the 2017–2020 ComSense Lab Maria de Maeztu Project, the Academic Director of the Consortium for Future Urban Mobility (Carnet), and the Chairman of the EIT-Urban Mobility European Association. He has authored more than 200 scientific and technical articles, reports, and chapters in specialized volumes. His current research interests include antennas, electromagnetic scattering and imaging, and system miniaturization for wireless, and sensing industrial and bio-applications from microwaves to terahertz frequencies.